




Comparing fundraising campaigns in healthcare using psychophysiological data: a network-based approach

Spyros Balafas^{1,6} · Clelia Di Serio¹ · Riccardo Lolatto² · Marco Mandolfo³ · Anna Maria Bianchi⁴ · Ernst Wit⁵ · Chiara Brombin¹ 

Accepted: 6 July 2024

© The Author(s), under exclusive licence to Società Italiana di Statistica 2024

Abstract

Measuring the effectiveness of fundraising campaigns is crucial for improving communication strategies. This is particularly pertinent for healthcare campaigns aimed at raising awareness about sensitive health issues that require financial support for advancing research efforts. The present work assesses campaign effectiveness by examining brain activation evoked by different video stimuli. Within a multivariate statistical setting, we compare the physiological responses that are induced by four fundraising campaigns designed under different communication strategies. Specifically, we model attention-related electroencephalographic (EEG) signals using graphical models to estimate partial correlation networks associated with each video campaign. These networks are then compared in terms of structure and connectivity using resampling methods. The proposed approach is flexible, allowing for the analysis of induced physiological responses at both local and global levels. It accounts for the interrelationships among collected EEG data and participants' heterogeneity, overcoming the need to derive composite scores as is commonly done in neuromarketing research areas. The networks derived from different campaigns exhibit significantly different structures and connectivity, indicating distinct cognitive and emotional responses induced by the videos. Given its generality, our proposed approach can be applied effectively in psychological and neuroscientific research fields whenever the physiological response to affective stimuli is of interest.

Extended author information available on the last page of the article

Published online: 29 July 2024

stimuli often involves the analysis of participants' psychophysiological responses, both subjectively and objectively (Mustafizur et al. 2021).

In this research, campaign effectiveness is assessed by leveraging electroencephalography (EEG) signals, which represent a valuable tool in the study of brain activity and function (Michel and Murray 2012). Notably, the brain operates as a network of functionally interconnected regions (Pessoa 2014), and EEG allows us to characterize these functional networks by utilizing various connectivity metrics (Chiarion et al. 2023; Lai et al. 2018). The connectivity within brain networks has been linked to behavioral functioning (Anzolin et al. 2017; Bosl et al. 2011). For instance, alterations in network connectivity have been associated with conditions such as epilepsy (Centeno and Carmichael 2014), reduced network connectivity has been observed in cases of mild cognitive impairment (Tóth et al. 2014) and aging (Hou et al. 2018; Javaid et al. 2022). In contrast, increased connectivity has been correlated with reduced math anxiety (Klados et al. 2019) and freezing of gait in Parkinson's disease patients (Asher et al. 2021).

The EEG signals considered in this study were obtained from an experimental research project designed to explore the objective physiological and subjective emotional responses to four videos from healthcare campaigns. The campaigns aimed to raise funds from the public to support research on rare diseases, and they were implemented with diverse communication strategies, including variations in narrators (internal or external) and subject matter. To assess the impact of each campaign, we use EEG signals associated with attention to estimate brain networks and subsequently investigate their connectivity as a proxy measure for effectiveness. According to the literature, attention, as a cognitive domain preserved throughout evolution, plays a fundamental role in the human cognitive system. We concentrate on attention since it enables the selection of behaviorally relevant information, prioritizing sensory processing and decision-making (Sreenivasan and Sridharan 2019). In this study, we assume that more effective campaigns will elicit increased attention and more interconnected networks (Contò et al. 2021; Domakonda et al. 2019; Weber et al. 2018). Thus, connectivity differences in the networks may reflect attention differences across campaigns. The dataset comprises recordings over time from electrodes spatially distributed across the participants' scalp, capturing local electrical oscillations in the brain during the video.

From a statistical perspective, time series methods represent an appealing computational tool to model EEG data (Gasser and Molinari 1996; Pardey et al. 1996). For instance, the (multivariate) autoregressive model has been used to formulate Granger causality tests (Granger 1969) for computing effective connectivity from partial direct temporal effects between electrodes or regions of interest (Goyal and Garg 2020; Khan et al. 2023; Phang et al. 2019). In more complex settings, advanced regression techniques such as the (generalized) linear mixed model (LMM, Pinheiro and Bates 2000) have been used to model simultaneously EEG recordings from multiple subjects (Frömer et al. 2018; Meinardi et al. 2023; Mir et al. 2022; Spinnato et al. 2015).

In designs where the linearity assumption is not satisfied, generalized additive models (GAMs, Wood 2017) have been proposed as a tool to model nonlinear characteristics in EEG data using smoothing splines (Eliseyev and Aksenova 2014;

Khare and Acharya 2023; Kryuchkova et al. 2012; Zhang et al. 2022). Typically, for modelling EEG networks multivariate approaches in the class of probabilistic graphical models (Lauritzen 1996; Whittaker 1990) are exploited (Schelter et al. 2006; Qiao et al. 2019; Li and Solea 2018). For modelling undirected EEG networks, Markov Random Fields (MRFs) are regularly used (Liu et al. 2016; Salazar et al. 2021). When the data fulfill the Gaussian assumption, the Gaussian graphical model (GGM) and its extensions have been applied to model undirected networks from EEG data (Gao et al. 2019; Min et al. 2022; Paz-Linares et al. 2023; Solea and Li 2022).

In this paper, we explore differences in brain connectivity induced by campaign exposures from a multivariate statistical perspective. The proposed approach integrates additive mixed models with GGMs to infer EEG networks from hierarchically structured multivariate time series data. Following this, to assess campaign efficacy, we examine the structural characteristics of the inferred EEG networks through pairwise comparisons in post-hoc analysis, employing resampling techniques with adjustments for multiple testing.

The paper is organized as follows. In Sect. 2 we discuss the EEG data collection process together with the experimental design. In the same section, we describe the psychometric tools used to investigate the subjective emotional experience, as well as the psychological scales administered to account for internalizing symptoms and personality traits of the participants in the analysis. The proposed statistical framework for modelling the experimental EEG data and the post-hoc tests for comparing the estimated EEG networks are discussed in detail in Sect. 3. The analysis results are presented in Sect. 4. Findings are discussed in Sect. 5.

2 Materials

2.1 Experimental design and data collection

The modelling approach is based on data generated by a collaborative effort between interdisciplinary groups¹. The study protocol was approved by the Ethics Committee of Politecnico di Milano (#31/2019).

Four videos, denoted as video 1, video 2, video 3, and video 4, from the campaign “Adotta il futuro” by the [Telethon Foundation](#), an Italian non-profit organization recognized by the Italian Ministry of Education, Universities, and Research for its active involvement in supporting research on rare genetic diseases, were analyzed in this study. We chose Telethon campaign videos as they aim to raise awareness about health issues, particularly rare diseases, and encourage participation. Telethon campaigns exhibit variability in communication style and execution. Video pairs 1 and 2, and video pairs 3 and 4, each featured identical images and background music. Videos 2 and 4 utilized internal

¹ [CUSBB](#): University Center for Statistics in the Biomedical Sciences, Vita-Salute San Raffaele University. [PHEEL](#): Physiology Emotion Experience Laboratory, Politecnico di Milano.

Table 1 Demographic information for the Telethon data

# Participants	Video 1 N = 14	Video 2 N = 21	Video 3 N = 16	Video 4 N = 23	Total N = 74
Age	27 (25, 43.75)	24 (23, 41)	25.5 (23.75, 40)	25 (23, 43)	25.5 (23, 41)
Gender	F: 9 (64.3%)	10 (47.6%)	8 (50.0%)	13 (56.5%)	40 (54.1%)
	M: 5 (35.7%)	11 (52.4%)	8 (50.0%)	10 (43.5%)	34 (45.9%)
TAS-20 score	37 (33.25, 44)	49 (46, 55)	48 (35, 59)	46 (37.5, 50)	46 (36, 54.75)
State anxiety	33 (30.25, 35.75)	34 (31, 39)	34.5 (32, 37.5)	31 (28, 37.5)	33.5 (30, 37)
Trait anxiety	36 (31.75, 38.75)	42 (32, 50)	42 (36.5, 51.25)	40 (34.5, 45)	39.5 (34, 46.75)

For categorical variables (i.e. gender) we calculate the frequency and the relative frequency, while for continuous variables the median together with the first (Q1) and third (Q3) quantiles

narrators, specifically a father or mother addressing the audience directly and sharing real-life stories of other parents with children afflicted by rare diseases. In contrast, videos 1 and 3 presented similar information on rare diseases and patients' quality of life through a disembodied "voice" external to the story world.

To compare the videos in terms of elicited emotional and physiological responses, serving as a proxy measure of video effectiveness, we evaluate EEG signals recorded during video viewing. Additionally, within the same protocol, other parts of autonomic nervous system (ANS) activity, such as heart rate variability skin electrical conductivity, and facial expression data, were collected throughout the video administration process. To further investigate the emotional experience provoked by the advertisements and assess anxiety and alexithymia constructs, self-report questionnaires were administered. Furthermore, health literacy regarding rare diseases and Telethon brand awareness were investigated, with preferences for the presented videos.

Experimental sessions were conducted at PHEEL on the Bovisa campus in Milan, from December 6–18, 2019 to February 3–7, 2020. During these sessions, 74 healthy adults aged between 19 and 64 participated in the experimental setup. Participants were randomly assigned to one of four groups, ensuring balance in age and gender distribution. Each group was tasked with watching two video campaigns, distinguished by the images used and the type of narrator. To mitigate habituation and learning effects, participants viewed either the sequence of videos 1 and 4 or 2 and 3, with the presentation order randomized within each sequence. However, for this study, we focused solely on measurements collected during the administration of the first video to prevent potential carry-over learning effects associated with evaluating the second video. Consequently, the analysis considered four independent groups of participants, corresponding to the four videos. Specifically, 14 participants viewed video 1 (18.9%), 21 viewed video 2 (28.4%), 16 viewed video 3 (21.6%), and 23 viewed video 4 (31.1%). Participant characteristics are summarized in Table 1.

2.2 Measuring subjective emotional experience

Emotional experiences were assessed using different psychometric scales, based on either discrete (Ekman 1992; Panksepp 1982, 2004) or dimensional (Russell 1980; Russell and Barrett 1999; Russell and Bullock 1985) theories of emotions. Following the video presentations, participants were asked to rate the intensity of six basic emotions—happiness, anger, fear, sadness, disgust, and surprise—on a 7-point Likert scale. Afterward, participants completed the Italian version of the differential emotion scale (DES, Battacchi et al. 1993; Izard et al. 1974; Schaefer et al. 2010), consisting of 16 items, each comprising a triplet of adjectives (e.g., “interested, concentrated, alert”). For each item, participants rated on a 7-point scale (ranging from 1=“not at all” to 7=“very intense”) the extent to which they experienced the described emotional state while watching the advertisements. Additionally, the Self-Assessment Manikin (SAM; Bradley and Lang, 1994) was utilized to gauge the valence and arousal induced by the videos, employing a 9-point pictorial scale.

Concerning the DES items, nearly all videos were considered engaging, with the item “interested, concentrated, alert” receiving the highest ratings. Participants also reported feeling “moved”, “sad, downhearted, blue”, and “loving, affectionate, friendly”. Notably, only participants who watched video 1 rated sadness lower than love. Nevertheless, there were no significant differences among the four videos in the scores obtained from the DES and SAM scales, indicating that, subjectively, the advertisements evoked similar emotional responses (Kruskal–Wallis test). The most prevalent emotions represented across all groups were interested, moved, sad, and loving, as illustrated in Fig. 1.

2.3 EEG: measuring emotional activation

EEG signals measure small electrical oscillations of just a few microvolts spontaneously generated in the brain cortex, reflecting various brain conditions. Oscillatory activity within different frequency ranges has been associated with diverse processes in the brain. Commonly utilized frequency ranges include δ (0.1–4 Hz), θ (4–8 Hz), α (8–13 Hz), β (13–36 Hz), and γ (above 36 Hz). In this study, we specifically focused on α (8–13 Hz) brain waves, as they have been correlated with affective and cognitive attention. The brain activity of each participant was recorded using the BE Plus LTM system, comprising 25 electrodes spatially distributed across the participant’s scalp according to the standard 10–20 configuration (Klem et al. 1999).

The EEG activity was collected at a sampling rate of 128 Hz, and the impedance level at the skin interface was maintained below 5 k Ω for all electrodes. EEG traces were automatically segmented to separate EEG activity recorded during the baseline period from that acquired during the observation of the videos. Pre-processing of the recorded EEG data included band-pass filtering (1–35 Hz), manual rejection of

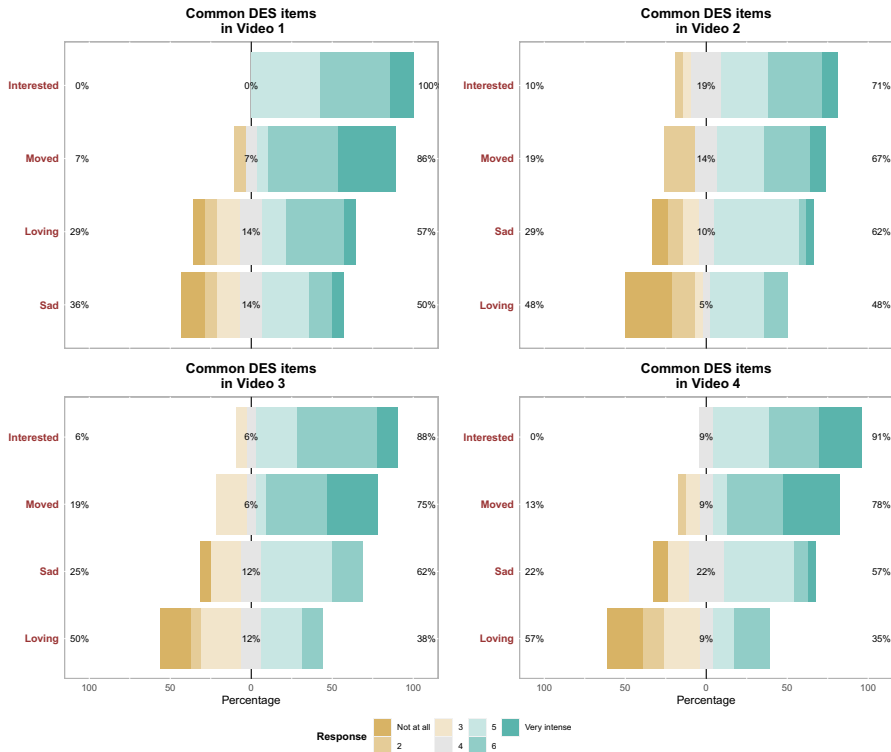


Fig. 1 Percentage distribution of the ratings for the four most relevant DES items within each video. For each bar of the Likert plots, on the left side the cumulative percentage of ratings below or equal to 3 is reported, in the middle the percentage of ratings for the neutral category 4 “Neither little nor intensely” is displayed, while on the right the cumulative percentage of ratings higher than or equal to 5 is shown

excessively corrupted epochs, and the execution of independent component analysis (ICA) to detect and remove components related to eye and muscular artifacts.

Furthermore, the EEG signal, referenced to a specific electrode positioned on the pre-cabled cap between CPz and Pz positions, was re-referenced using the common average reference (CAR) method. This re-referencing technique aims to minimize uncorrelated sources of signal and noise through averaging while eliminating noise sources common to all sites.

The signal was decomposed into typical frequency bands. The individual alpha frequency (IAF) was identified for each subject during the baseline period, and the alpha rhythm was extracted using an FIR digital filter centered on the IAF with a bandwidth of 4 Hz. This filtering process was applied with zero phase, Kaiser windowing, and an order of 800. To quantify alpha power, the squared single samples of the filtered signal were computed, and the resulting series was averaged over non-overlapping time windows of 0.5 s. This approach allowed for characterizing alpha power dynamics across the EEG recordings.

2.4 Psychological scales

Validated self-report questionnaires were administered to assess anxiety, which has been linked with EEG activity (Blackhart et al. 2006), and alexithymia, characterized by difficulty in identifying and describing emotions. At the outset of the experiment, participants completed the State-Trait Anxiety Inventory (STAY-Y Pedrabissi and Santinello 1989; Spielberger et al. 1983), which comprises 40 items in total, with 20 items measuring trait anxiety (STAI-1) and 20 measuring state anxiety (STAI-2). Responses were rated on a 4-point Likert-type scale ranging from 1=“almost never” to 4=“almost always”. Each scale yielded a total score ranging from 20 to 80, with higher scores indicating elevated anxiety levels. A cut-off point of 40 is commonly employed to indicate anxiety symptoms (Barisone et al. 2004).

Additionally, participants completed the Toronto Alexithymia Scale (TAS-20 Bagby et al. 1994; Bressi et al. 1996), consisting of 20 items rated on a 5-point Likert scale ranging from 1=“strongly disagree” to 5=“strongly agree”. The TAS-20 measures three factors: difficulty identifying feelings, describing feelings to others, and externally oriented thinking.

Median scores on the TAS, STAI, and STAI-Y scales for each group are displayed in Table 1. TAS-20 scores were below the cut-off value ($TAS \geq 61$) for the presence of alexithymia, and STAI scores were below the threshold ($STAI \geq 41$) for anxiety symptoms, except for the trait anxiety score of participants who viewed videos 2 and 3. For these participants, the median STAI score was 42, indicating mild anxiety.

Participants randomized to watch the four videos obtained significantly different scores in total TAS (Kruskal–Wallis $\chi^2 = 8.6227$, $p = 0.03475$). Specifically, post-hoc analysis revealed a significant difference in the scores obtained by participants assigned to watch videos 1 and 2 (Dunn’s post-hoc comparison test with a Bonferroni correction for multiple testing, $p_{Bonf} = 0.0213$).

3 Methods

This study proposes to model EEG networks with undirected edges by assuming symmetric relationships between the electrodes. Undirected graphical models, also known as Markov random fields (MRFs), represent families of distributions that adhere to a set of conditional independence relationships among the random variables, depicted by an undirected graph \mathcal{G} . A graph is defined as a pair $\mathcal{G} = (\mathcal{V}, \mathcal{E})$, where $\mathcal{V} = \{1, \dots, p\}$ denotes the set of vertices or nodes, and $\mathcal{E} \subseteq \mathcal{V} \times \mathcal{V}$ represents the set of edges. In this context, we adopt a Gaussian MRF, called Gaussian graphical model (GGM).

The GGM is a multivariate approach that entails a Gaussian random vector with additional conditional independencies, or Markov properties. Let $\mathbf{Y}_{\mathcal{V}} = (Y_1, \dots, Y_p)^T$ denote a vector of random variables indexed by the set of vertices associated with electrodes in the study, where each $Y_j, j \in \mathcal{V}$, represents a vector with n observations

Moreover, assume that the random vector $\mathbf{Y}_{\mathcal{V}}$ is generated from a p -variate Gaussian distribution,

$$\mathbf{Y}_V \sim \mathcal{N}_p(\boldsymbol{\mu}, \boldsymbol{\Sigma}), \tag{1}$$

with a $p \times 1$ mean vector $\boldsymbol{\mu} = (\mu_1, \dots, \mu_p)^T$ and a symmetric $p \times p$ covariance matrix $\boldsymbol{\Sigma}$ with inverse $\boldsymbol{\Theta} = \boldsymbol{\Sigma}^{-1}$, which is known as precision or concentration matrix. The data \mathbf{Y}_V are typically centred before the analysis, and the mean vector $\boldsymbol{\mu}$ is fixed to zero.

In a GGM, the sparsity pattern in the precision matrix $\boldsymbol{\Theta}$ corresponds to conditional independence statements represented by the graph \mathcal{G} . This arises from the pairwise Markov property, which states that two distinct vertices $i, j \in \mathcal{V}$ in the graph with $i \neq j$, are conditionally independent given the rest,

$$Y_i \perp Y_j \mid \mathbf{Y}_{\mathcal{V} \setminus \{i,j\}} \Leftrightarrow \omega_{ij} = -\frac{\theta_{ij}}{\sqrt{\theta_{ii}\theta_{jj}}} = 0,$$

where θ_{ij} denotes the (i, j) -th element of the precision matrix $\boldsymbol{\Theta}$. Thus, estimating the structure of a GGM involves a covariance selection task (Dempster 1972), where one estimates the sparse inverse covariance matrix of a multivariate Gaussian distribution, with non-zero elements associated with edges in \mathcal{G} . Estimating $\boldsymbol{\Theta}$ under any framework that induces sparsity in the parameter space such as the graphical LASSO (gLASSO, Friedman et al. 2007), or any other regularized neighborhood selection method (Meinshausen and Bühlmann 2006) yields a GGM representation.

The traditional GGM parametrization in Eq. (1) assumes that all observations are generated independently from a common multivariate Gaussian distribution. However, in more complex settings, such as hierarchical longitudinal data, the traditional GGM may not adequately capture the various sources of heterogeneity and multiple dependencies inherent in real data. To address this limitation and accommodate the heterogeneity present in multivariate time series data from individuals nested within different groups, we propose a hierarchical GGM approach (HGGM). This approach allows for the specification of a distinct network structure for each group of participants, thereby enabling more flexible data modelling.

3.1 Hierarchical Gaussian graphical model

Consider an EEG study involving n participants indexed by $i \in \{1, \dots, n\}$, who are randomized into V different groups, denoted by $v \in \{1, \dots, V\}$, where $n = \sum_{v=1}^V n_v$. Each participant from group v is assigned to watch a distinct fundraising video campaign. During the video presentation, the brain activity of each participant i from group v is measured simultaneously at each time point $t \in \{1, \dots, T\}$ from p electrodes spatially distributed across the scalp, indexed by $j \in \mathcal{V}$, where $\mathcal{V} = \{1, \dots, p\}$ represents the vertex set of a graph \mathcal{G} .

Let $\mathbf{y} = \{y_{vijt}\}$ represent the data from the study, with the EEG activity measured on person i in group v , electrode j , and time t . The vector of measurements $\mathbf{y}_{vit} = (y_{vit1}, \dots, y_{vitp})^T$ for person i in group v at time t is p -dimensional and is modelled as,

$$\begin{aligned}
\mathbf{y}_{vit} \mid \mathbf{Q}_i &\sim \mathcal{N}_p(\boldsymbol{\mu}_{vit}, \boldsymbol{\Sigma}_v) \\
\boldsymbol{\mu}_{vit} &= \mathbf{a}_v + \mathbf{B}\mathbf{x}_{it} + \mathbf{f}(\mathbf{w}_{it}) + \mathbf{Q}_i\mathbf{z}_{it} \\
\mathbf{Q}_i &\sim \mathcal{MN}_{p \times l}(\mathbf{0}_{p \times l}, \mathbf{I}_{p \times p}, \boldsymbol{\Sigma}_Q) \\
\boldsymbol{\epsilon}_{vit} &\sim \mathcal{N}_p(\mathbf{0}, \boldsymbol{\Sigma}_v)
\end{aligned} \tag{2}$$

where $\boldsymbol{\mu}_{vit} = (\mu_{vit1}, \dots, \mu_{vitp})^\top$ is a p -variate vector of person and video-specific means, and $\boldsymbol{\Sigma}_v$ is a $p \times p$ video specific-covariance matrix with inverse $\boldsymbol{\Theta}_v = \boldsymbol{\Sigma}_v^{-1}$. The vectors \mathbf{x}_{it} , \mathbf{w}_{it} , \mathbf{z}_{it} are of dimensions m , d , and l respectively corresponding to the t -th row of known model matrices for the fixed, smooth, and random covariates from person i . Moreover, \mathbf{a}_v is a vector of video-specific intercepts, \mathbf{B} is a $p \times m$ matrix for the fixed effects, $\mathbf{f}(\cdot) = (f_1(\cdot), \dots, f_p(\cdot))^\top$ is a p -dimensional vector of arbitrary smooth functions, and \mathbf{Q}_i is a $p \times l$ matrix with the person—specific random effects. The random effects follow a matrix normal distribution, with independent rows and column covariance $\boldsymbol{\Sigma}_Q = \text{bdiag}(\boldsymbol{\Sigma}_1(Q), \dots, \boldsymbol{\Sigma}_p(Q))$ a block diagonal matrix with $l \times l$ dimensional blocks $\boldsymbol{\Sigma}_j(Q)$ on its diagonal. By including only random intercepts in the model, then $\mathbf{z}_{it} = z_{it} = 1$, $l = 1$, $\mathbf{Q}_i = \mathbf{q}_i = (q_{i1}, \dots, q_{ip})^\top$ becomes a $p \times 1$ vector of random effects, and $\boldsymbol{\Sigma}_Q$ is reduced to a large diagonal matrix parametrized by a p -dimensional vector of variance parameters, i.e., $\boldsymbol{\Sigma}_Q = \text{diag}(\sigma_1^2(Q), \dots, \sigma_p^2(Q))$.

3.2 Estimation procedure

The parameters of the hierarchical GGM described in Eq. (2) are estimated by a two-stage procedure. In the first step the p -dimensional person specific means $\boldsymbol{\mu}_{vit} = (\mu_{vit1}, \dots, \mu_{vitp})^\top$ are estimated from their univariate counterparts. Then, the residuals from the first step model are modelled in a second step to estimate the video-specific inverse covariance matrix $\boldsymbol{\Theta}_v$, which encodes the graph structure.

3.2.1 First step: univariate estimation of the person-specific means

The person-specific mean vector $\boldsymbol{\mu}_{vit}$ is estimated through a univariate electrode-by-electrode estimation procedure. This involves independently estimating each row of the matrices \mathbf{B} and \mathbf{Q}_i , along with each component of the smooth functional vector $\mathbf{f}(\cdot)$. To accomplish this, we assume that the matrix $\boldsymbol{\Sigma}$ from Eq. (2) is a diagonal matrix with p variances σ_j^2 on its diagonal. Thus, in the first step, the mean from each person i , campaign v , and electrode j , is modelled by a univariate additive mixed model with random intercepts. That is,

$$\begin{aligned}
 y_{vijt} \mid q_{ij} &\sim N\left(\mu_{vijt}, \sigma_j^2\right) \\
 \mu_{vijt} &= a_{vj} + \mathbf{x}_{it}^T \boldsymbol{\beta}_j + z_{it}^T q_{ij} + f_j(\mathbf{w}_{it}^T) \\
 q_{ij} &\sim N\left(0, \sigma_j^2(Q)\right) \\
 \epsilon_{vijt} &\sim N\left(0, \sigma_j^2\right)
 \end{aligned} \tag{3}$$

where \mathbf{x}_{it}^T , \mathbf{z}_{it}^T , and \mathbf{w}_{it}^T are the same as in (2), $\boldsymbol{\beta}_j$ is an $m \times 1$ vector of fixed effects corresponding to the j^{th} row of \mathbf{B} , and q_{ij} is the j -th element of the $p \times 1$ vector \mathbf{q}_i . Estimating the group and time-varying person specific mean for electrode j , $\hat{\mu}_{vijt}$ thus implies estimating the fixed effect parameters $\boldsymbol{\beta}_j$, the thin plate regression spline function $f_j(\cdot)$ (Wood 2003), the random effect q_{ij} together with its variance $\sigma_j^2(Q)$, and the error variance σ_j^2 . In practice, the parameters of the additive mixed model described in (3) can be estimated using a Bayesian framework implemented in the function `gam()`, which is available in the R package `mgcv` (Wood 2017).

3.2.2 Second step: regularized neighborhood selection

In the second step, we consider the residuals from the first-step model in Eq. (3). Let $\epsilon_{vijt} = y_{vijt} - \hat{\mu}_{vijt}$ be the residual from person i in group v , electrode j , and time t . Let $\epsilon_v = (\epsilon_{v1}, \dots, \epsilon_{vp})^T$ collect the residual observations from all participants in group v . The ϵ_v is assumed to follow a p -variate normal distribution,

$$\epsilon_v \sim \mathcal{N}_p(\mathbf{0}, \boldsymbol{\Theta}_v^{-1}) \tag{4}$$

where the video-specific mean vector common to all individuals in the group v , $\boldsymbol{\mu}_v$, is fixed to zero, and $\boldsymbol{\Theta}_v$ is the inverse of the covariance matrix $\boldsymbol{\Sigma}_v$. The precision matrix $\boldsymbol{\Theta}_v$ associated with the underlying graph \mathcal{G} is assumed to be sparse encoding all the conditional independencies between the electrodes.

For estimating the precision matrix $\boldsymbol{\Theta}_v$ we employ the gLASSO (Friedman et al. 2007) algorithm, which solves the following minimization problem:

$$\min_{\boldsymbol{\Theta}_v \in \mathbb{S}_{++}^p} -\log \det(\boldsymbol{\Theta}_v) + \text{trace}(\mathbf{S}_v \boldsymbol{\Theta}_v) + \lambda \|\boldsymbol{\Theta}_v\|_1, \tag{5}$$

where \mathbb{S}_{++}^p is the cone of symmetric positive definite matrices of size $p \times p$, $\text{trace}(\cdot)$ corresponds to the trace operator of a matrix, \mathbf{S}_v is the $p \times p$ sample covariance matrix of ϵ_v , λ is a positive regularization parameter that shrinks the off-diagonal elements of $\boldsymbol{\Theta}_v$ towards zero, and $\|\cdot\|_1$ is the sum of absolute values of the off-diagonal elements of $\boldsymbol{\Theta}_v$.

The optimal regularization parameter λ is determined by minimizing information criteria. In this work, we consider the extended Bayesian Information Criterion (EBIC, Foygel and Drton 2010) for GGMs, which is defined as,

$$EBIC(\lambda) = -2\ell_{N_v}(\hat{\boldsymbol{\Theta}}_v(\lambda)) + \hat{\mathcal{E}}_v(\lambda) \log(N_v) + 2\hat{\mathcal{E}}_v(\lambda) \log(p) \tag{6}$$

where $\mathcal{E}_v(\lambda)$ is equal to the edge set associated with the estimate of Θ_v for a particular λ , $N_v = n_v T$ is the number of observations, $\ell_{N_v}(\hat{\Theta}_v(\lambda))$ denotes the value of the log-likelihood function for the model associated with the parameter λ , and p is the cardinality of the vertex set.

3.3 Post-hoc network comparison

The ultimate goal of this study is to compare networks estimated by the hierarchical GGM presented in Sect. 3.1. Since the normality assumption underlying standard statistical tests cannot be justified in penalized regression settings (Pötscher and Leeb 2009), Van Borkulo et al. (2022) proposed a nonparametric permutation-based test called the network comparison test (NCT). The NCT is implemented in the R package **NetworkComparisonTest** (van Borkulo 2015). NCT is designed for comparing undirected graphs on three structural aspects, and its algorithm consists of three steps.

1. *Network estimation* In the first step, it estimates the network structure for each group and subsequently calculates the test statistic. Network estimation can be performed using various graph estimation algorithms (here we use the gLASSO).
2. *Reference distribution* In the second step, the algorithm creates the reference distribution of the test statistic by repeatedly sampling the observed data based on the original sample size, re-estimating the network structure in each repetition, and recalculating the test statistic.
3. *Significance evaluation* In the last step, NCT evaluates the significance of the test statistic from the first step by comparing it to the reference distribution created in the second step.

The NCT approach can test the difference between networks both at the global and local levels. Specifically, the tests that can be performed involve hypotheses regarding:

1. *Invariant network structure* (global level).
2. *Invariant connectivity strength* (global level).
3. *Invariant edge strength* (local level).

In this study, we focus on global network differences, which means that we restrict ourselves to connectivity tests that involve the hypothesis of invariant connectivity strength (2.).

Let \mathcal{G}_1 and \mathcal{G}_2 be the undirected graphs from two GGMs, each consisting of the same p variables. These graphs (networks) are characterized by the $p \times p$ symmetric precision matrices Θ_1 and Θ_2 respectively. These matrices consist of elements θ_{ij}^k , $k \in \{1, 2\}$ with the regression weight between nodes i and j , where $i, j \in \mathcal{V}$ and $i \neq j$. When there is no edge connecting two nodes i and j , then these nodes are conditionally independent and $\theta_{ij}^k = 0$.

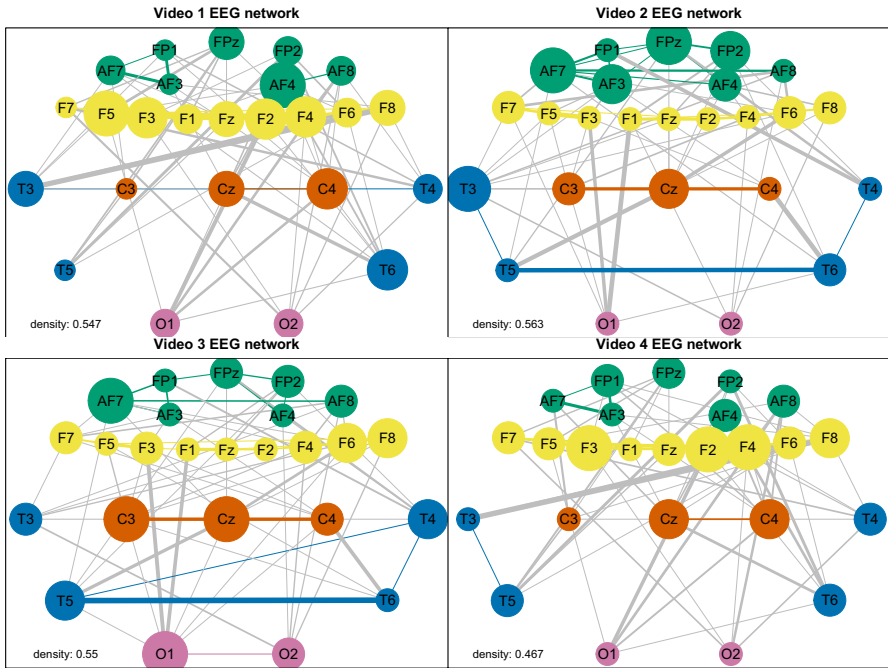


Fig. 2 Undirected networks for each group in the study, with their corresponding network density on the bottom left corner of each figure. Grey edges connect electrodes from different groups, while colored edges connect electrodes of the same group. For the sake of interpretability edges with absolute weight lower than 0.05 are not shown in the graphs (colour figure online)

The test on invariant connectivity strength tests the following hypothesis:

$$H_0 : \sum_{i=1}^p \sum_{j>i} |\theta_{ij}^1| = \sum_{i=1}^p \sum_{j>i} |\theta_{ij}^2| \text{ (the global connectivity strength is equal),}$$

$$H_1 : \sum_{i=1}^p \sum_{j>i} |\theta_{ij}^1| \neq \sum_{i=1}^p \sum_{j>i} |\theta_{ij}^2| \text{ (the global connectivity strength is not equal),}$$

using the test statistic:

$$S(\theta_{ij}^1 - \theta_{ij}^2) = \left| \sum_{i=1}^p \sum_{j>i} |\theta_{ij}^1| - \sum_{i=1}^p \sum_{j>i} |\theta_{ij}^2| \right|.$$

The resulting *p*-value of the test is the proportion of samples that have a test statistic larger than that of the observed data.

4 Results

Initially, participant-specific means are modelled using fixed effects such as a first-order autoregressive effect and baseline electrode activity. These fixed effects also include participants’ demographic and psychological characteristics, such as age,

gender, TAS, and STAI scores. The functional part of the model captures any time variation in average electrode activity at the population level. Finally, the random part of the model accounts for person-specific variability with a normally distributed random intercept. In the second step, we fit a GGM to the residuals obtained from the first-level mean model, specifically focusing on video-specific residuals.

4.1 Estimated networks and network descriptive statistics

Figure 2 shows the estimated networks for each video. The networks are densely connected, and thus hard to describe by visual inspection. However, overall network connectivity may be summarized by computing network density, a global network statistic indicating the proportion of present over possible edges in the network. It takes values between 0 and 1 and the higher the density the more connected is the network. The most densely connected network corresponds to video 2 ($\text{density}_2 = 0.563$) followed by video 3 ($\text{density}_3 = 0.55$). The networks that correspond to videos 1 and 4 are less dense, with $\text{density}_1 = 0.547$ and $\text{density}_4 = 0.467$ respectively.

Local network descriptive statistics at the electrode (node) level were utilized to characterize the estimated network structures. Specifically, degree, closeness, and betweenness centralities were examined. Each centrality index captures different aspects of network connectivity. Degree centrality, the simplest measure to compute, indicates the number of edges connected to a node. Closeness (Bavelas 1950) and betweenness (Freeman 1977) centralities are based on the concept of shortest path and have been widely used to characterize EEG networks (van Straaten and Stam 2013; Ferri et al. 2007). The standardized centrality indices are visualized in Fig. 3. The dark orange circle represents the center of the centrality distribution. Centrality values higher or lower than the dark orange circle indicate more or less central electrodes in the network. Electrode names highlighted in blue are situated on the midline of the scalp, those in green correspond to electrodes in the right hemisphere, and those in red are on the left hemisphere of the scalp.

Figure 3 reveals similar patterns across all centrality indices. Examining the degree centrality, we observe that in the video 1 network, 10 electrodes exhibit centrality higher than the average. The most central electrode is F4, followed by F8, T3, and T5 with the same degree. Among these 10 central electrodes, three (30%) are situated in the right hemisphere of the brain, one (10%) is at the midline, and six (60%) are in the left hemisphere. Additionally, six central electrodes (60%) are positioned in the frontal part of the brain.

In the video 2 EEG network, 13 electrodes demonstrate centrality above the average. The most central electrode is F6, followed by F8 and T5. Among these 13 central electrodes, six (46.15%) are located in the right hemisphere, one (7.69%) is at the midline, and six (46.15%) are in the left hemisphere. Moreover, six out of the 13 central electrodes (46.15%) are situated in the frontal part of the brain.

In the video 3 EEG network, 11 electrodes exhibit higher than average degree centrality. The most central electrodes are F7 and T6. Among these 11 central electrodes, four (36.36%) are positioned in the right hemisphere, two (18.18%) are

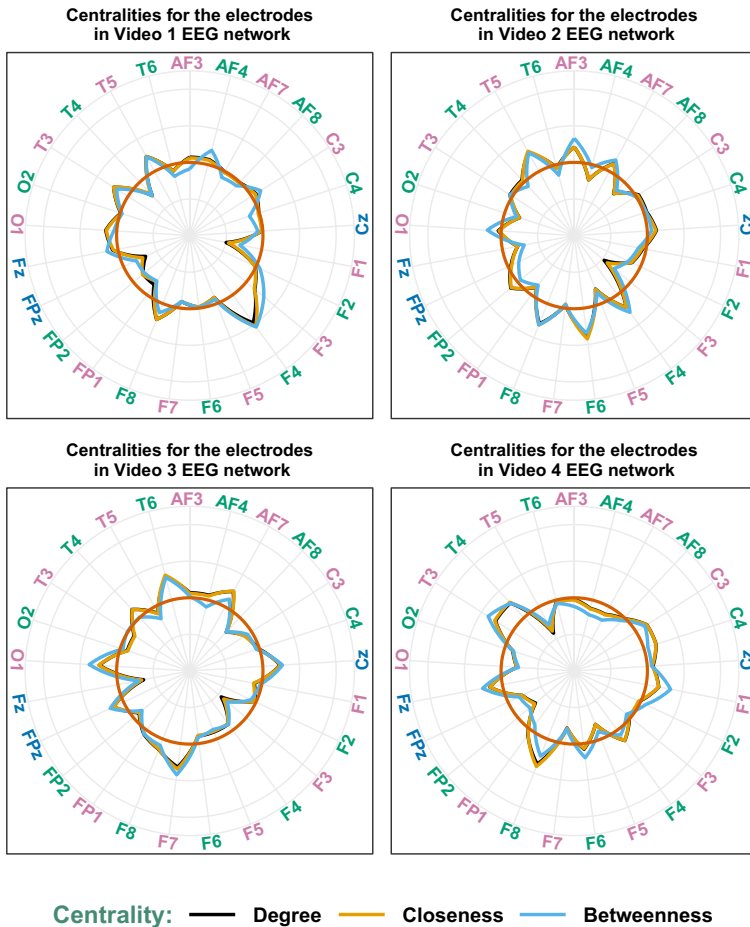


Fig. 3 Standardized node centrality indices for the estimated networks. The orange circle corresponds to zero. Electrodes located at the right hemisphere of the scalp are colored green, electrodes located at the left hemisphere of the scalp are colored red, and electrodes located at the center of the scalp are colored blue. Degree centrality is shown in black, closeness centrality in yellow, and betweenness centrality in blue (colour figure online)

at the midline, and five (45.45%) are in the left hemisphere. Additionally, seven electrodes (63.63%) out of the 11 central electrodes are located in the frontal part of the brain.

In the video 4 network, 11 electrodes are central higher than average. The most central electrodes in this network are F8, followed by T3 and T4. Among these 11 central electrodes, five (45.45%) are situated in the right hemisphere, two (18.18%) are at the midline, and four (36.36%) are in the left hemisphere. Additionally, six of these central electrodes (54.54%) are located in the frontal part.

Topographic maps generated from EEG data, known as topoplots, offer valuable insights into brain activity distribution across different regions. These maps

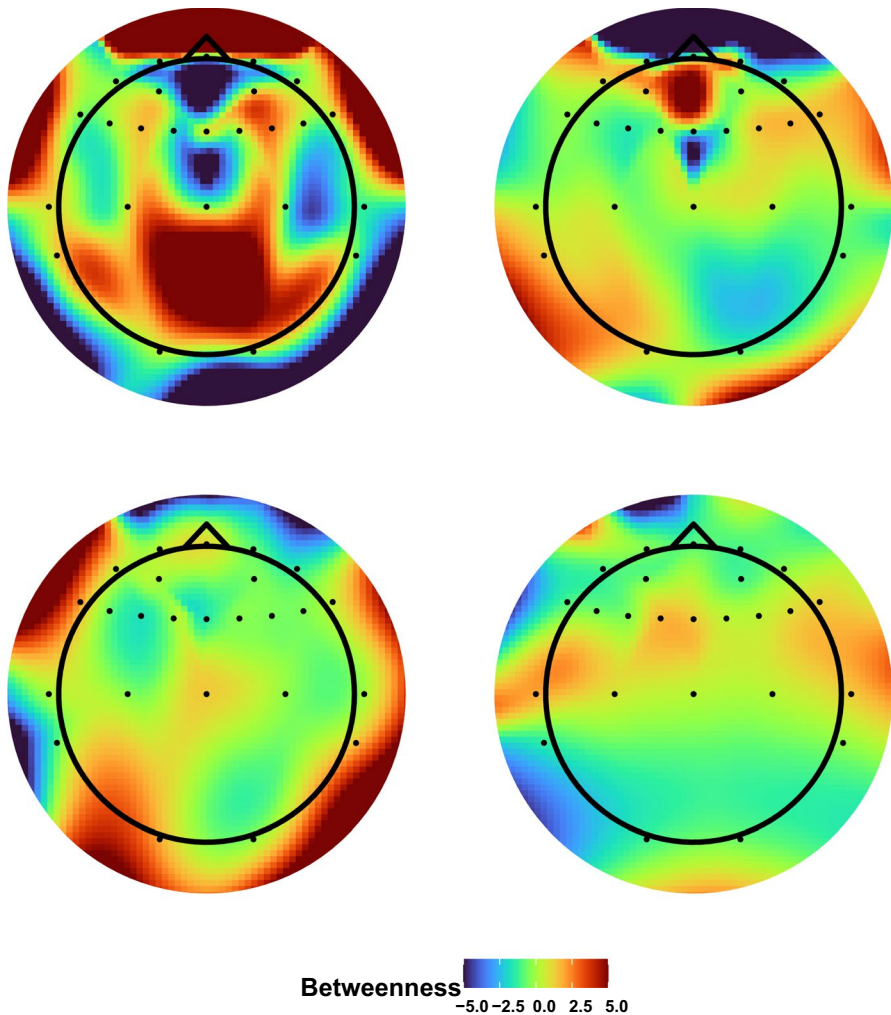


Fig. 4 Topographic map of an EEG field as a 2-D circular view (looking down at the top of the head) that visualizes the standardized electrode betweenness centrality for each estimated network. Red color corresponds to high betweenness centrality and blue corresponds to low betweenness centrality. The topoplots linked with videos 1 and 2 are showcased in the upper left and right panels, respectively, while those associated with videos 3 and 4 are displayed in the bottom left and right panels (colour figure online)

visualize the activation of various brain areas, allowing researchers to identify patterns associated with distinct cognitive functions. Given the study's objective of identifying more engaging campaigns, attention is typically directed towards the frontal part of the brain, which plays a crucial role in attentional processes.

By plotting topoplots focusing on the frontal region, researchers can observe the distribution of centrality indices or other relevant metrics across electrodes.

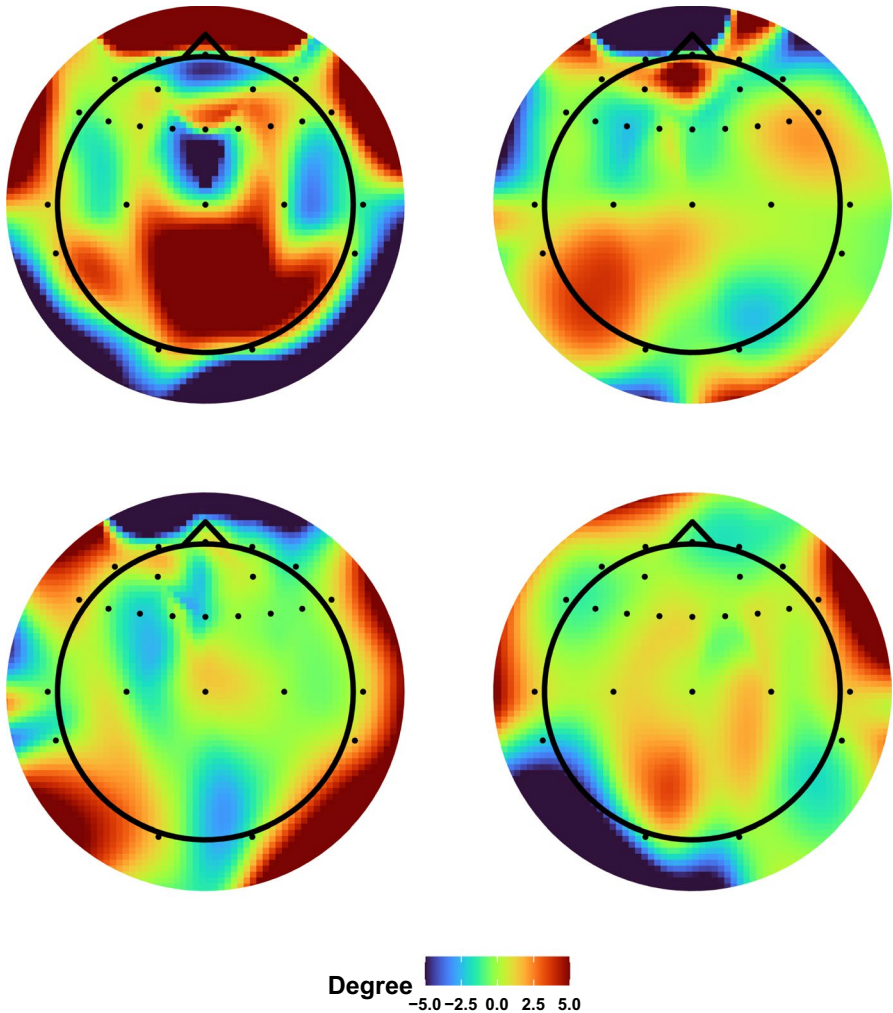


Fig. 5 Topographic map of an EEG field as a 2-D circular view (looking down at the top of the head) that visualizes the standardized electrode degree centrality for each estimated network. Red colour corresponds to a high degree centrality and blue corresponds to a low degree centrality. Topoplots associated with video 1 and 2 are shown respectively in the upper left and right panels, while maps associated with video 3 and 4 are displayed in the bottom left and right panels (colour figure online)

This visualization helps in understanding how different stimuli or conditions affect attention-related brain activity. Areas with higher centrality or activity levels may indicate increased engagement or processing of information related to the stimulus, suggesting stronger attentional involvement.

Figures 4 and 5 provide insightful topoplots illustrating centrality patterns across different brain regions for each video campaign. These topoplots

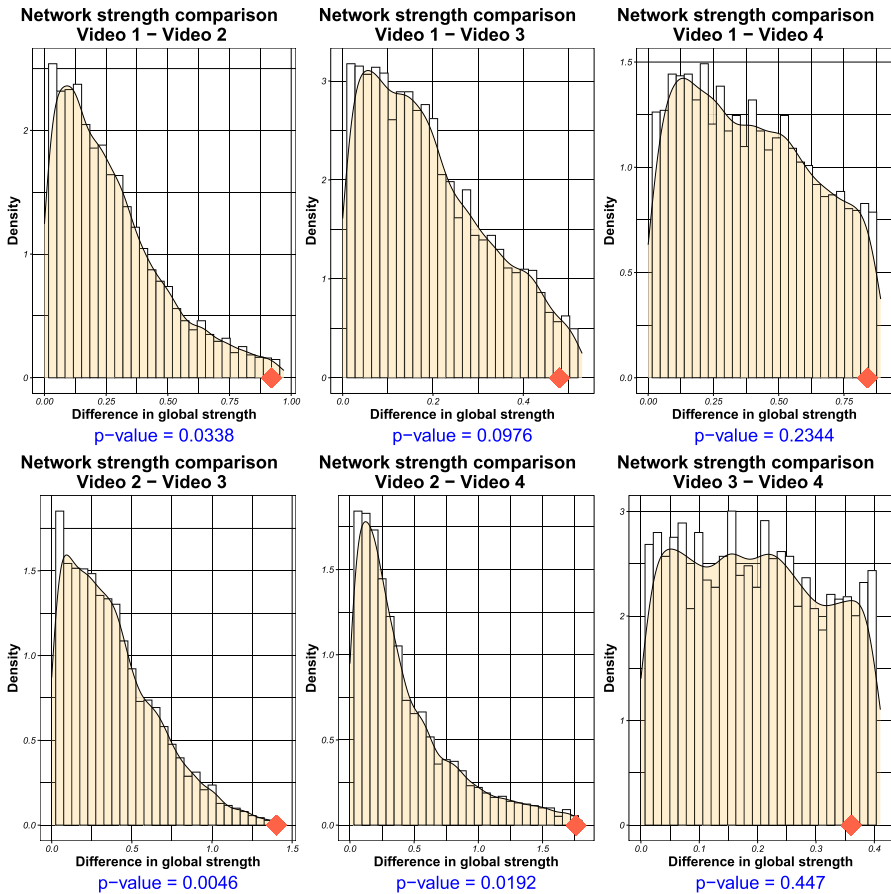


Fig. 6 Results of the test on network connectivity. Each plot corresponds to a pairwise video comparison and shows the distribution of the test statistic. The red diamond-shaped point corresponds to the value of the observed test statistic. The resulting p -value of the test is shown in blue (colour figure online)

are constructed based on betweenness and degree centralities, offering a comprehensive view of how different videos elicit distinct neural responses.

In both figures, regions with high centrality values, indicating greater activation, are depicted in red, while regions with lower activation are shown in blue. Consistent centrality patterns are observed for each video, highlighting the unique neural signatures associated with them.

Looking at video 1, (in the upper left part of both figures), it's evident that this video triggers widespread activation across the brain, particularly in the frontal region associated with attentional processes. Video 2, depicted in the upper right of the figures, exhibits significant activation in the frontal region, albeit in a more localized area than video 1.

On the other hand, videos 3 and 4, represented in the bottom left and right panels respectively, show distinct centrality patterns. While both videos elicit high

activation, especially in the brain hemispheres, they demonstrate less pronounced activation in the frontal region compared to videos 1 and 2.

These findings indicate that different videos result in networks with different structural characteristics, brain activation intensity, and spatial distribution across regions. This enhances our understanding of how diverse stimuli impact cognitive processes, especially attention, crucial for video advertising effectiveness.

4.2 Network comparisons

The NCT approach was used to compare the estimated networks, focusing primarily on identifying differences in overall connectivity strength. By conducting such analyses, we can discern whether certain videos elicit distinct neural responses compared to others, shedding light on the effectiveness of video content in engaging specific brain regions and cognitive processes.

Figure 6 displays the NCT results on network connectivity strength, providing insights into the pairwise comparisons between the estimated networks for each video campaign. The plots in the panel illustrate the p -values obtained from the pairwise network comparisons. Notably, comparisons involving the network from the second video campaign exhibit p -values below the significance threshold ($\alpha = 0.05$). Specifically, significant connectivity differences were observed between:

1. The first and second campaign ($S_{12} = 0.9204204$, $p = 0.0338$).
2. The second and third campaign ($S_{23} = 1.400741$, $p = 0.0046$).
3. The second and fourth campaign ($S_{24} = 1.761043$, $p = 0.0192$).

These findings suggest that the second video campaign induces distinct neural connectivity patterns compared to the other campaigns. However, no significant connectivity differences were detected between the other campaign pairs.

5 Discussion

This study introduces a comprehensive methodological framework for comparing alternative fundraising campaigns and assessing the impact of corresponding videos on cognitive functions. Focusing on four fundraising campaigns, EEG data were modelled using undirected graphical models. Specifically, hierarchical GGMs were employed to capture the heterogeneity in multivariate time series. The structures of the resulting networks were compared using nonparametric testing procedures, under the assumption that more effective campaigns would lead to higher attention and denser networks (Orquin and Wedel 2020; Venkatraman et al. 2015).

The results revealed that the second fundraising campaign yielded the most densely connected network. Moreover, the network comparison indicated significantly higher connectivity for the second fundraising campaign compared to the others. Thus, under the assumption that more effective campaigns would result in more connected EEG networks, the second fundraising campaign

emerged as the most effective among the four. Analysis of participants' preferences suggested that videos featuring an internal narrator (second and fourth videos) were more likely (66.2%) to enhance donation compared to others. This finding aligns with the network analysis results from EEG data, suggesting that characters or actors speaking directly to the audience convey messages more effectively.

This study introduces a novel data-driven approach to evaluating fundraising campaign effectiveness, which can be extended to analyze other affective stimuli. Integrating both self-reported emotional experiences and objective physiological activation within analogous study structures can yield valuable insights. Such an approach allows for a comprehensive analysis, enabling the identification of stylistic elements that contribute to the effectiveness and engagement of campaigns. By combining subjective perceptions with objective physiological responses, researchers can gain a deeper understanding of the emotional experiences and reactions elicited by fundraising campaigns. It is worth noting that the nature of this study primarily leans towards an exploratory perspective. This exploratory approach is instrumental in fostering a holistic understanding of emotional experiences and reactions to fundraising campaigns.

Importantly, the proposed approach eliminates the need to rely on composite indicators, as conclusions are based on the entire connectivity structure derived directly from raw EEG data. Furthermore, this method allows for a straightforward graphical representation of the conditional dependence structure, providing valuable insights into brain activation in specific areas.

Studies encompassing a larger sample size and addressing possible sources of confounding could improve the generalizability of our findings. For example, examining socio-demographic factors can reveal how variables like age, gender, education, and socioeconomic status influence emotional processing and subsequent behavior. Understanding the interplay between psychological factors and emotional processing is crucial, as it sheds light on how individuals perceive and respond to stimuli.

Other possible educational features that affect the perception of health-related topics should be considered. In particular, differences in health literacy levels can impact how individuals interpret and act upon emotional messages. Additionally, familiarity with both the advertisement and the topic can influence habituation and learning effects, thus affecting emotional responses. Analyzing the consistency between self-reported intentions and actual behavior is vital for understanding the efficacy of emotional stimuli. Considering potential biases like social desirability can provide valuable insights into the reliability of self-reported data. Moreover, when starting the experimental session, an assessment was conducted on alexithymia and anxiety traits, both involved in emotion processing. However, as we have emphasized the role of attention in campaign effectiveness, it could be interesting to assess and account for attention abilities using psychometric tools.

Overall, integrating these elements into future research can provide a comprehensive understanding of how individual characteristics shape affective responses

and subsequent behaviors, offering valuable implications for various fields such as marketing, psychology, and public health.

Data availability The data that support the findings of this study and the code for reproducing the results are openly available in “Zenodo” at <https://doi.org/10.5281/zenodo.7940926>, version v1.0.0.

References

- Anzolin A, Mattia D, Toppi J, Pichiorri F, Riccio A, Astolfi L (2017) Brain connectivity networks at the basis of human attention components: an EEG study. In: 2017 39th annual international conference of the IEEE engineering in medicine and biology society (EMBC), p 3953–3956
- Asher EE, Plotnik M, Günther M, Moshel S, Levy O, Havlin S, Bartsch RP (2021) Connectivity of EEG synchronization networks increases for Parkinson’s disease patients with freezing of gait. *Commun Biol* 4:1017. <https://doi.org/10.1038/s42003-021-02544-w>
- Bagby RM, Parker JD, Taylor GJ (1994) The twenty-item Toronto Alexithymia Scale-I. Item selection and cross-validation of the factor structure. *J Psychosom Res* 38(1):23–32. [https://doi.org/10.1016/0022-3999\(94\)90005-1](https://doi.org/10.1016/0022-3999(94)90005-1)
- Barisone M, Lerda S, Ansaldi S, De Vincenzo E, Angelini G (2004) Psychopathology and epilepsy: clinical experience in a centre for the diagnosis and care of epilepsy. *J Psychopathol* 10(3):336
- Battacchi M, Suslow T, Renna M, Cavallero C (1993) Uno studio di validazione fattoriale della versione Italiana della differential emotions scale. *Riv Psicol Clin* 7(1):23–39
- Bavelas A (1950) Communication patterns in task-oriented groups. *J Acoust Soc Am* 22(6):725–730. <https://doi.org/10.1121/1.1906679>
- Blackhart GC, Minnix JA, Kline JP (2006) Can EEG asymmetry patterns predict future development of anxiety and depression?: A preliminary study. *Biol Psychol* 72(1):46–50. <https://doi.org/10.1016/j.biopsycho.2005.06.010>
- Bosl W, Tierney A, Tager-Flusberg H, Nelson C (2011) EEG complexity as a biomarker for autism spectrum disorder risk. *BMC Med* 9:18. <https://doi.org/10.1186/1741-7015-9-18>
- Bradley MM, Lang PJ (1994) Measuring emotion: the self-assessment manikin and the semantic differential. *J Behav Ther Exp Psychiatry* 25(1):49–59. [https://doi.org/10.1016/0005-7916\(94\)90063-9](https://doi.org/10.1016/0005-7916(94)90063-9)
- Bressi C, Taylor G, Parker J, Bressi S, Brambilla V, Aguglia E et al (1996) Cross validation of the factor structure of the 20-item Toronto Alexithymia Scale: an Italian multicenter study. *J Psychosom Res* 41(6):551–559. [https://doi.org/10.1016/s0022-3999\(96\)00228-0](https://doi.org/10.1016/s0022-3999(96)00228-0)
- Centeno M, Carmichael DW (2014) Network connectivity in epilepsy: resting state FMRI and EEG-FMRI contributions. *Front Neurol* 5:93. <https://doi.org/10.3389/fneur.2014.00093>
- Chiarion G, Sparacino L, Antonacci Y, Faes L, Mesin L (2023) Connectivity analysis in EEG data: a tutorial review of the state of the art and emerging trends. *Bioengineering* 10(3):372. <https://doi.org/10.3390/bioengineering10030372>
- Contò F, Edwards G, Tyler S, Parrott D, Grossman E, Battelli L (2021) Attention network modulation via tRNS correlates with attention gain. *eLife* 10:63782. <https://doi.org/10.7554/eLife.63782>
- Dempster AP (1972) Covariance selection. *Biometrics* 28(1):157–175. <https://doi.org/10.2307/2528966>
- Domakonda MJ, He X, Lee S, Cyr M, Marsh R (2019) Increased functional connectivity between ventral attention and default mode networks in adolescents with bulimia nervosa. *J Am Acad Child Adolesc Psychiatry* 58(2):232–241. <https://doi.org/10.1016/j.jaac.2018.09.433>
- Ekman P (1992) Are there basic emotions? *Psychol Rev* 99(3):550–553. <https://doi.org/10.1037/0033-295x.99.3.550>
- Eliseyev A, Aksenova T (2014) Stable and artifact-resistant decoding of 3d hand trajectories from ECoG signals using the generalized additive model. *J Neural Eng* 11(6):066005. <https://doi.org/10.1088/1741-2560/11/6/066005>
- Ferri R, Rundo F, Bruni O, Terzano MG, Stam CJ (2007) Small-world network organization of functional connectivity of EEG slow-wave activity during sleep. *Clin Neurophysiol* 118(2):449–456. <https://doi.org/10.1016/j.clinph.2006.10.021>

- Foygel R, Drton M (2010) Extended Bayesian information criteria for Gaussian graphical models. In: Lafferty J, Williams C, Shawe-Taylor J, Zemel R, Culotta A (eds) *Advances in neural information processing systems*, vol 23. Curran Associates, Inc
- Freeman LC (1977) A set of measures of centrality based on betweenness. *Sociometry* 40(1):35–41. <https://doi.org/10.2307/3033543>
- Friedman J, Hastie T, Tibshirani R (2007) Sparse inverse covariance estimation with the graphical lasso. *Biostatistics* 9(3):432–441. <https://doi.org/10.1093/biostatistics/kxm045>
- Frömer R, Maier M, Abdel Rahman R (2018) Group-level EEG-processing pipeline for flexible single trial-based analyses including linear mixed models. *Front Neurosci* 12:48. <https://doi.org/10.3389/fnins.2018.00048>
- Gao X, Shen W, Ting C-M, Cramer SC, Srinivasan R, Ombao H (2019) Estimating brain connectivity using copula gaussian graphical models. In: 2019 IEEE 16th international symposium on biomedical imaging (ISBI 2019), p 108–112
- Gasser T, Molinari L (1996) The analysis of the EEG. *Stat Methods Med Res* 5(1):67–99. <https://doi.org/10.1177/096228029600500105>
- Goyal A, Garg R (2020) Effective EEG connectivity by sparse vector autoregressive model. In: *Proceedings of the 7th ACM IKDD CoDS and 25th COMAD*. Association for Computing Machinery, New York, NY, USA, p 37–45
- Granger CWJ (1969) Investigating causal relations by econometric models and cross-spectral methods. *Econometrica* 37(3):424–438. <https://doi.org/10.2307/1912791>
- Gross G, Huber G, Klosterkötter J, Linz M (2013) BSABS: Bonner skala für die beurteilung von basis-symptomen bonn scale for the assessment of basic symptoms manual, kommentar, dokumentationsbogen. Springer-Verlag, Berlin
- Hou F, Liu C, Yu Z, Xu X, Zhang J, Peng C-K, Yang A (2018) Age-related alterations in electroencephalography connectivity and network topology during n-back working memory task. *Front Hum Neurosci* 12:484. <https://doi.org/10.3389/fnhum.2018.00484>
- Izard C, Dougherty F, Bloxom B, Kotsch N (1974) The differential emotions scale: a method of measuring the subjective experience of discrete emotions. Vanderbilt University, Nashville
- Javaid H, Kumarnsit E, Chatpun S (2022) Age-related alterations in EEG network connectivity in healthy aging. *Brain Sci* 12(2):218. <https://doi.org/10.3390/brainsci12020218>
- Khan DM, Yahya N, Kamel N, Faye I (2023) A novel method for efficient estimation of brain effective connectivity in EEG. *Comput Methods Progr Biomed* 228:107242. <https://doi.org/10.1016/j.cmpb.2022.107242>
- Khare SK, Acharya UR (2023) An explainable and interpretable model for attention deficit hyperactivity disorder in children using EEG signals. *Comput Biol Med* 155:106676. <https://doi.org/10.1016/j.compbiomed.2023.106676>
- Klados MA, Paraskevopoulos E, Pandria N, Bamidis PD (2019) The impact of math anxiety on working memory: a cortical activations and cortical functional connectivity EEG study. *IEEE Access* 7:15027–15039. <https://doi.org/10.1109/ACCESS.2019.2892808>
- Klem G, Lüders HO, Jasper HH, Elger C (1999) The ten-twenty electrode system of the international federation. In: *Recommendations for the practice of clinical neurophysiology: guidelines of the international federation of clinical physiology* (EEG suppl. 52). Elsevier Science B.V
- Kostygina G, Tran H, Binns S, Szczypka G, Emery S, Vallone D, Hair E (2020) Boosting health campaign reach and engagement through use of social media influencers and memes. *Soc Media+ Soc* 6(2):2056305120912475. <https://doi.org/10.1177/2056305120912475>
- Kryuchkova T, Tucker BV, Wurm LH, Baayen RH (2012) Danger and usefulness are detected early in auditory lexical processing: evidence from electroencephalography. *Brain Lang* 122(2):81–91. <https://doi.org/10.1016/j.bandl.2012.05.005>
- Lai M, Demuru M, Hillebrand A, Fraschini M (2018) A comparison between scalp-and source-reconstructed EEG networks. *Sci Rep* 8:12269. <https://doi.org/10.1038/s41598-018-30869-w>
- Lauritzen SL (1996) *Graphical models*. Clarendon Press, Lauritzen, UK
- Li B, Solea E (2018) A nonparametric graphical model for functional data with application to brain networks based on fMRI. *J Am Stat Assoc* 113(524):1637–1655. <https://doi.org/10.1080/01621459.2017.1356726>
- Liu K, Yu ZL, Wu W, Gu Z, Li Y, Nagarajan S (2016) Bayesian electromagnetic spatio-temporal imaging of extended sources with Markov random field and temporal basis expansion. *Neuroimage* 139:385–404. <https://doi.org/10.1016/j.neuroimage.2016.06.027>

- Meinardi VB, López JMD, Fajreldines HD, Boyallian C, Balzarini M (2023) Linear mixed-effect models for correlated response to process electroencephalogram recordings. *Cogn Neurodyn*. <https://doi.org/10.1007/s11571-023-09984-6>
- Meinshausen N, Bühlmann P (2006) High-dimensional graphs and variable selection with the lasso. *Ann Stat* 34(3):1436–1462. <https://doi.org/10.1214/009053606000000281>
- Michel CM, Murray MM (2012) Towards the utilization of EEG as a brain imaging tool. *Neuroimage* 61(2):371–385. <https://doi.org/10.1016/j.neuroimage.2011.12.039>
- Min K, Mai Q, Zhang X (2022) Fast and separable estimation in high-dimensional tensor gaussian graphical models. *J Comput Graph Stat* 31(1):294–300. <https://doi.org/10.1080/10618600.2021.1938086>
- Mir M, Nasirzadeh F, Bereznicki H, Enticott P, Lee S (2022) Investigating the effects of different levels and types of construction noise on emotions using EEG data. *Build Environ* 225:109619. <https://doi.org/10.1016/j.buildenv.2022.109619>
- Mustafizur R, Ajay KS, Amzad H, Selim H, Rabiul I, Biplob H, Mohammad AM (2021) Recognition of human emotions using EEG signals: a review. *Comput Biol Med* 136:104696. <https://doi.org/10.1016/j.combiomed.2021.104696>
- Orquin JL, Wedel M (2020) Contributions to attention based marketing: foundations, insights and challenges. *J Bus Res* 111:85–90. <https://doi.org/10.1016/j.jbusres.2020.02.012>
- Panksepp J (1982) Toward a general psychobiological theory of emotions. *Behav Brain Sci* 5(3):407–422. <https://doi.org/10.1017/S0140525X00012759>
- Panksepp J (2004) *Affective neuroscience: the foundations of human and animal emotions*. Oxford University Press, Oxford
- Pardey J, Roberts S, Tarassenko L (1996) A review of parametric modelling techniques for EEG analysis. *Med Eng Phys* 18(1):2–11. [https://doi.org/10.1016/1350-4533\(95\)00024-0](https://doi.org/10.1016/1350-4533(95)00024-0)
- Paz-Linares D, Gonzalez-Moreira E, Areces-Gonzalez A, Wang Y, Li M, Martinez-Montes E, Valdes-Sosa PA (2023) Identifying oscillatory brain networks with hidden Gaussian graphical spectral models of m EEG. *Sci Rep* 13(1):11466. <https://doi.org/10.1038/s41598-023-38513-y>
- Pedrabissi L, Santinello M (1989) Verifica della validità dello stai forma y di spielberger. *Bollet Psicol Appl* 191–192:11–14
- Pessoa L (2014) Understanding brain networks and brain organization. *Phys Life Rev* 11(3):400–435. <https://doi.org/10.1016/j.plev.2014.03.005>
- Phang C-R, Ting C-M, Samdin SB, Ombao H (2019) Classification of EEG-based effective brain connectivity in schizophrenia using deep neural networks. In: 2019 9th international IEEE/EMBS conference on neural engineering (NER), p 401–406
- Pinheiro JC, Bates DM (2000) *Mixed-effects models in S and S-plus*. Springer, New York, NY
- Pötscher BM, Leeb H (2009) On the distribution of penalized maximum likelihood estimators: the LASSO, SCAD and thresholding. *J Multivar Anal* 100(9):2065–2082. <https://doi.org/10.1016/j.jmva.2009.06.010>
- Qiao X, Guo S, James GM (2019) Functional graphical models. *J Am Stat Assoc* 114(525):211–222. <https://doi.org/10.1080/01621459.2017.1390466>
- Russell JA (1980) A circumplex model of affect. *J Pers Soc Psychol* 39(6):1161–1178. <https://doi.org/10.1037/h0077714>
- Russell JA, Barrett LF (1999) Core affect, prototypical emotional episodes and other things called emotion: dissecting the elephant. *J Pers Soc Psychol* 76(5):805–19. <https://doi.org/10.1037/0022-3514.76.5.805>
- Russell JA, Bullock M (1985) Multidimensional scaling of emotional facial expressions: similarity from preschoolers to adults. *J Pers Soc Psychol* 48(5):1290–1298. <https://doi.org/10.1037/0022-3514.48.5.1290>
- Salazar A, Vergara L, Safont G (2021) Generative adversarial networks and Markov random fields for oversampling very small training sets. *Expert Syst Appl* 163:113819. <https://doi.org/10.1016/j.eswa.2020.113819>
- Schaefer A, Nils F, Sanchez X, Philippot P (2010) Assessing the effectiveness of a large database of emotion-eliciting films: a new tool for emotion researchers. *Cogn Emot* 24(7):1153–1172. <https://doi.org/10.1080/02699930903274322>
- Schelter B, Winterhalder M, Hellwig B, Guschlbauer B, Lücking CH, Timmer J (2006) Direct or indirect? Graphical models for neural oscillators. *J Physiol-Paris* 99(1):37–46. <https://doi.org/10.1016/j.jphysparis.2005.06.006>
- Solea E, Li B (2022) Copula Gaussian graphical models for functional data. *J Am Stat Assoc* 117(538):781–793. <https://doi.org/10.1080/01621459.2020.1817750>

- Speilberger C, Gorsuch R, Lushene R, Vagg P, Jacobs G (1983) Manual for the state-trait anxiety inventory (form y)("self-evaluation questionnaire"). Consulting Psychologists, Palo Alto, CA
- Spinnato J, Roubaud M-C, Burle B, Torrésani B (2015) Detecting single-trial EEG evoked potential using a wavelet domain linear mixed model: application to error potentials classification. *J Neural Eng* 12(3):036013. <https://doi.org/10.1088/1741-2560/12/3/036013>
- Sreenivasan V, Sridharan D (2019) Subcortical connectivity correlates selectively with attention's effects on spatial choice bias. *Proc Natl Acad Sci* 116(39):19711–19716. <https://doi.org/10.1073/pnas.1902704116>
- Tóth B, File B, Boha R, Kardos Z, Hidasi Z, Gaál ZA, Molnár M (2014) EEG network connectivity changes in mild cognitive impairment—preliminary results. *Int J Psychophysiol* 92(1):1–7. <https://doi.org/10.1016/j.ijpsycho.2014.02.001>
- van Borkulo CD (2015) Package 'networkcomparisontest' [Computer software manual]
- Van Borkulo CD, van Bork R, Boschloo L, Kossakowski JJ, Tio P, Schoevers RA, Waldorp LJ (2022) Comparing network structures on three aspects: a permutation test. *Psychol Methods* 28(6):1273–1285. <https://doi.org/10.1037/met0000476>
- van Straaten EC, Stam CJ (2013) Structure out of chaos: functional brain network analysis with EEG, MEG and functional MRI. *Eur Neuropsychopharmacol* 23(1):7–18. <https://doi.org/10.1016/j.euronuro.2012.10.010>
- Venkatraman V, Dimoka A, Pavlou PA, Vo K, Hampton W, Bollinger B, Winer RS (2015) Predicting advertising success beyond traditional measures: new insights from neurophysiological methods and market response modeling. *J Mark Res* 52(4):436–452. <https://doi.org/10.1509/jmr.13.0593>
- Weber R, Alicea B, Huskey R, Mathiak K (2018) Network dynamics of attention during a naturalistic behavioral paradigm. *Front Hum Neurosci* 12:182. <https://doi.org/10.3389/fnhum.2018.00182>
- Whittaker J (1990) Graphical models in applied multivariate statistics. Wiley, New York, NY
- Wood S (2003) Thin plate regression splines. *J R Stat Soc Ser B Stat Methodol* 65(1):95–114. <https://doi.org/10.1111/1467-9868.00374>
- Wood S (2017) Generalized additive models: an introduction with R, 2nd edn. Chapman and Hall/CRC, New York
- Zhang X, Fang K, Zhang Q (2022) Multivariate functional generalized additive models. *J Stat Comput Simul* 92(4):875–893. <https://doi.org/10.1080/00949655.2021.1979550>

Publisher's Note Springer Nature remains neutral with regard to jurisdictional claims in published maps and institutional affiliations.

Springer Nature or its licensor (e.g. a society or other partner) holds exclusive rights to this article under a publishing agreement with the author(s) or other rightsholder(s); author self-archiving of the accepted manuscript version of this article is solely governed by the terms of such publishing agreement and applicable law.

Authors and Affiliations

Spyros Balafas^{1,6} · **Clelia Di Serio**¹ · **Riccardo Lolatto**² · **Marco Mandolfo**³ · **Anna Maria Bianchi**⁴ · **Ernst Wit**⁵ · **Chiara Brombin**¹ 

✉ Chiara Brombin
brombin.chiara@hsr.it

¹ University Center for Statistics in the Biomedical Sciences (CUSBS), Università Vita-Salute San Raffaele, Via Olgettina, 58, Milan 20132, Italy

² Division of Infectious Diseases, IRCCS San Raffaele Scientific Institute, Via Olgettina, 58, 20132 Milan, Italy

³ Department of Management, Economics, and Industrial Engineering, Politecnico di Milano, Via Raffaele Lambruschini, 4/B, 20156 Milan, Italy

⁴ Department of Electronics, Information Science and Bioengineering, Politecnico di Milano, Via Giuseppe Ponzio, 34, 20133 Milan, Italy

⁵ Institute of Computing, Università della Svizzera italiana, Via la Santa, 1, 6962 Lugano, Switzerland

⁶ Groningen Research Institute of Pharmacy, Unit of Pharmacotherapy, -Epidemiology and -Economics, University of Groningen, Antonius Deusinglaan 1, 9713 AV Groningen, The Netherlands